Science of the Total Environment 917 (2024) 170398

Contents lists available at ScienceDirect

Science of the Total Environment

journal homepage: www.elsevier.com/locate/scitotenv

Competitive heavy metal adsorption on pinecone shells: Mathematical modelling of fixed-bed column and surface interaction insights

Marwa Ben Amar [a], Maryam Mallek [a], Abel Valverde [b,c], Hèctor Monclús [d], Timothy G. Myers [e], Victoria Salvadó [f], Alba Cabrera-Codony [d,*]

[a] Laboratory of Material Sciences and Environment, Faculty of Science, University of Sfax, Tunisia
[b] Department of Chemical Engineering, Universitat Politècnica de Catalunya, 08028 Barcelona, Spain
[c] Visiting Fellow, Mathematical Institute, University of Oxford, Oxford OX2 6GG, UK
[d] LEQUIA (Institute of the Environment), University of Girona, C/M. Aurèlia Capmany, 69, Girona 17003, Spain
[e] Centre de Recerca Matemàtica, Bellaterra 08193, Spain
[f] Department of Chemistry, Faculty of Science, University of Girona, M. Aurèlia Capmany, 69, 17003 Girona, Spain

HIGHLIGHTS

- Adsorption capacities of 65 and 11 $mg \cdot g^{-1}$ for Pb(II) and Cu(II) were obtained.
- When Pb(II) competed with Cu(II) and Cd(II) the adsorption capacity was 23.8 $mg \cdot g^{-1}$.
- High correlation of the model with experimental data suggests surface complexation.
- FTIR and XRD confirm the functional groups' active involvement in metal adsorption.
- Robust column model gives valuable insights into adsorption kinetics and mechanisms.

GRAPHICAL ABSTRACT

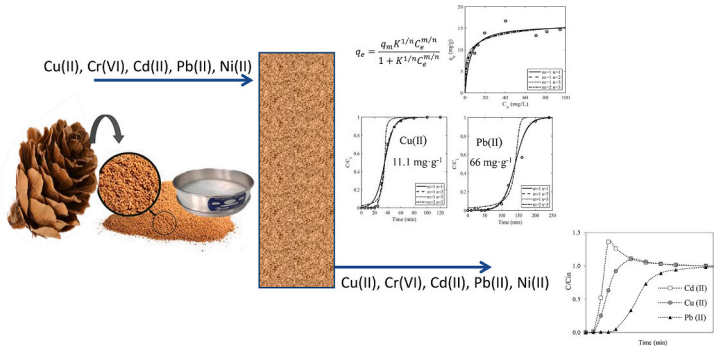

ARTICLE INFO

Editor: Damià Barceló

Keywords:
Heavy metals
Pinecone solid waste
Metal industry wastewater
Adsorption modelling

ABSTRACT

Pinecone shells are assessed as a cost-effective biosorbent for the removal of metal ions Pb(II), Cu(II), Cd(II), Ni (II), and Cr(VI) in a fixed-bed column. Influent concentration, bed height, and flowrate are studied to improve efficiency. The breakthrough data is well fitted by the Sips adsorption model, suggesting a surface complexation mechanism, with maximum adsorption capacities of 11.1 mg/g for Cu(II) and 66 mg/g for Pb(II).

In multimetal solutions, the uptake sequence at breakthrough and saturation is Pb(II) > Cu(II) > Cd(II). Characterization via FTIR and XRD reveals carboxyl and hydroxyl functional groups interacting with metal ions. Ca(II) does not compete with Pb(II), Cu(II), and Cd(II) adsorption, highlighting the ability of pinecone to adsorb heavy metals via surface complexation. Its application in the treatment of industrial effluents containing Cu(II), Ni(II), and Cr(VI) is explored.

The study investigates bed media regeneration via eluting adsorbed metal ions with hydrochloric acid solutions. The potential of pinecone shells as an efficient biosorbent for removing toxic metal ions from industrial wastewater is emphasized. These findings enhance our understanding of the adsorption mechanism and

* Corresponding author.
E-mail address: alba.cabrera@udg.edu (A. Cabrera-Codony).

https://doi.org/10.1016/j.scitotenv.2024.170398
Received 20 November 2023; Received in revised form 10 January 2024; Accepted 22 January 2024
Available online 27 January 2024

underscore the fixed-bed column system's applicability in real-world scenarios, addressing environmental concerns related to heavy metal contamination of industrial effluents.

1. Introduction

Industrial effluents containing high concentrations of heavy metals, arising from metal cleaning, plating, textile, and battery manufacturing processes, pose a grave environmental threat. The non-biodegradable nature of these metals and their propensity to bioaccumulate in living organisms necessitates the development of effective technologies for their removal before discharge (Li et al., 2024). In recent years, biosorption has emerged as an efficient, low-cost alternative to conventional methods such as chemical precipitation, coagulation/flocculation, ion exchange, and membrane processes for removing heavy metals such as Cu(II), Cd(II), Pb(II), and Cr(VI) (Malik et al., 2018). These conventional methods suffer from drawbacks, including high costs, sludge generation, and inefficiency at low metal concentrations.

In the practical operation of full-scale biosorption processes, continuous-flow fixed-bed columns and fluidized bed columns are often preferred to treat large volumes of effluent due to the large surface area per unit of volume that can be achieved, which results in a high mass transfer (Hethnawi et al., 2018). Lignocellulosic, agricultural, agroforestry, and agroindustry wastes have been recognized for their capacity to adsorb metal ions, which is attributed to their porous structures and diverse functional groups, such as carboxyl and hydroxyl, on their surfaces (Afroze and Sen, 2018; Kumar et al., 2023; Lakshmipathy and Sarada, 2016). In Circular Economy context (Cabrera-Codony et al., 2021), milled olive stone and pinecone shells, which are abundant and inexpensive agricultural waste in many Mediterranean countries, have demonstrated remarkable adsorption capacities for Pb(II), Cu(II), Cd(II), and Cr(VI) (Amar et al., 2021, 2020; Blázquez et al., 2011; Martín-Lara et al., 2016c; Ucun et al., 2003). The aforementioned studies have mostly been performed in batch mode under equilibrium conditions, providing information about the effectiveness of adsorbate-adsorbent systems and determining the maximum adsorption capacity. However, such data is not generally applicable to continuous adsorptive systems where there is insufficient contact time to reach equilibrium (Han et al., 2023; Zahara et al., 2023).

In previous fixed-bed column investigations, lignocellulosic biosorbents were explored to remove single metal ions such as Pb(II), Cu(II), Cd(II), and Cr(VI), as well as to treat multimetal solutions. Branches pruned from olive trees and pinecone shells were studied for Pb(II) biosorption in lab-scale fixed-bed columns, with an additional evaluation of Cu(II) and Pb(II) binary biosorption using pinecone shells (Martín-Lara et al., 2016a). Other agricultural residues such as grape stalk waste (Miralles et al., 2010), watermelon rind and spent coffee grains (Davila-Guzman et al., 2016), citrus peels (Chatterjee and Schiewer, 2014) and sugarcane bagasse (Vera et al., 2018) have also been assessed for their heavy metal adsorption capabilities.

Industrial effluents from electroplating processes contain heavy metals such as nickel, copper, zinc, chromium, lead, and cadmium (Rajoria et al., 2022). These effluents exceed the limits established by standard regulations and therefore require pre-treatment before discharge (BOE-A-1993-31103). Various biosorbents have proven effective in removing these metals from electroplating effluents, showing promise for environmental protection. Xanthated chitosan and plain chitosan flakes in a fixed-bed column were able to eliminate Cr(VI) from electroplating effluents (Chauhan and Sankararamakrishnan, 2011). Encapsulated *Moringa oleifera* was successfully applied to remove Zn(II), Cu(II), Mn(II), Co(II), and Ni(II) from electroplating wastewater (Radhakrishnan et al., 2016), whereas almond shell was able to adsorb Cu(II) and Cr(VI) from tannery wastewater (Yahya et al., 2020). Grape stalk waste demonstrated adsorption capacities of 56.11 $mg \cdot g^{-1}$ for Pb (II) and 33.12 $mg \cdot g^{-1}$ for Cd(II) in column experiments (Miralles et al., 2010). Other agricultural residues such as *Syzygium cumini* and *Populus deltoids* leaf powders were also found to be effective for removing Cu(II), Ni(II) and Cr(VI) from electroplating industrial effluents (Kaur et al., 2013).

The aim of the present study is to explore the potential of milled pinecone shells for the efficient removal of heavy metals in wastewater treatment across diverse industrial processes. The efficacy of this biosorbent has previously been demonstrated in the work (Amar et al., 2021). The adsorption capacity of milled pinecone shells from Tunisian agricultural waste was evaluated in a series of batch experiments, resulting in maximum adsorption capacities of 95 $mg \cdot g^{-1}$ for Pb(II), 33.55 $mg \cdot g^{-1}$ for Cu(II), and 50 $mg \cdot g^{-1}$ for Cd(II) at pH 5.4, and 68.03 $mg \cdot g^{-1}$ for Cr(VI) at pH 2. The investigation also involved a study of fixed-bed column data, indicating that Cu(II) and Cr(VI) adsorption is best approximated by a Langmuir isotherm while Pb(II) and Cb(II) follow a Langmuir-Freundlich model. It was also demonstrated that, at the low concentrations studied, there was little competition between the adsorption of different contaminants.

A main goal of the present study is to characterise the column adsorption process. Traditional approaches for characterization involve comparing a mathematical model for the breakthrough curve with experimental data and so inferring unknown parameters. However, these methods frequently encounter challenges when specific data segments deviate from the model, and fitted parameters violate fundamental model assumptions. This suggests that a new approach is required to understand the process and so aid in the development of more efficient and precise water treatment methods (Valverde et al., 2024). The approach adopted in the present work builds on the mathematical model developed by (Aguareles et al., 2023) which is based on the Sips adsorption isotherm. One of the key strengths of the Sips isotherm is its wide applicability, encompassing a number of standard isotherms (including Langmuir).

As well as applying a novel model to characterise the adsorption of single contaminant systems our study was extended to include the competitive adsorption of ternary metal solutions containing Pb(II), Cu(II), and Cd(II); to investigate the impact of Ca(II) in the solution; the removal of Cu(II) from an electronic industry effluent, and Cu(II), Ni(II) and Cr(VI) from electroplating effluents. Finally, the recyclability of pinecone shells was explored by performing desorption tests.

2. Materials and methods

2.1. Adsorbent material

The adsorbent material was obtained from pinecone shells agricultural waste sourced from Tunisia, a Mediterranean region with prolific production that can benefit from waste valorisation. The raw material was processed for use as an adsorbent. The pinecone shells were crushed and washed with distilled water. The samples were subsequently dried at 105 °C for 24 h to eliminate moisture. Dried samples were milled using a laboratory grinder and sieved to achieve a particle size <200 μm.

Table 1
Physical and chemical properties of pinecone shells.

BET surface area $[m^2 \cdot g^{-1}]$	0.2536
Particle size distribution	70 % <50 μm; 15.8 % <100 μm, 7 % <150 μm; 12.5 % >150 μm
pH_{pzc}	6.2
Surface elemental composition (EDX)	C: 53.48 %; O: 44.77 %; S: 0.17 %; Ca: 0.67 %

The particle size distribution showed that >70 % of the particles have a particle size <50 μm (Table 1). In general, smaller particle sizes result in a larger external surface facilitating the adsorption of the metal ions. The main physical and chemical properties of the biosorbent including analysis of surface area by BET micrometric measurements, and the pH at the point of zero charge were determined in our previous study (Amar et al., 2021) and are set out in Table 1.

2.2. Surface characterization

The milled and sieved pinecone shells adsorbent material obtained was fully characterized by scanning electron microscopy (SEM) (Model ZEISS DSM-960A) operated at 30 kV. The SEM was equipped with an energy-dispersive X-ray spectrometer Bruker Nano XFlash Detector 5010 to determine the surface composition of the material.

Fourier transformed infrared spectroscopy (FT-IR) of the pinecone shell samples was undertaken before and after metal extraction with a Perkin-Elmer Paragon 2000 FTIR spectrometer from 600 to 3600 cm^{-1} in order to characterise the functional groups in the surface of the adsorbent and identify the changes after metal adsorption.

XRD diffractograms using Cu Kα radiation ($\lambda = 1.54060$ Å) at 40 kV and 15 mA in the range of 2Θ from 5° to 70° (Bruker, Germany) before and after extraction were recorded to examine the crystalline structure of pinecone shells.

Samples of the exhausted adsorbent were removed from the glass column at the end of the adsorption test sand mixed to obtain a representative sample of the column as a whole for characterization.

2.3. Metal solutions and analytical procedures

Stock solutions of metals (Cu, Pb, Cd, Cr, and Ni) were prepared at a concentration of 1000 $mg{\cdot}L^{-1}$ by dissolving appropriate quantities of Cu $(NO_3)_2{\cdot}3H_2O$, $Pb(NO_3)_2$, $Cd(NO_3)_2{\cdot}4H_2O$, K_2CrO_4, and $Ni(NO_3)_2{\cdot}6H_2O$ (Panreac, Barcelona, Spain) in doubly deionized water (MilliQ) obtained from a Millipore water purification system (18.2 MΩ cm^{-1}, Millipore, Bedford, MA, USA). Intermediate and working metal solutions were prepared by dilution of the stock solutions with MilliQ water. A COBOS precision ATX-224 balance was employed to weigh the amounts of the reagents as well as of the adsorbents. To perform Cu(II) adsorption tests, a synthetic solution was prepared with a composition of: 123.94 $mg{\cdot}L^{-1}$ of Cu(II), 11.28 $mg{\cdot}L^{-1}$ of NO_3^-, 2.68 $mg{\cdot}L^{-1}$ of NO_2^-, 418.83 $mg{\cdot}L^{-1}$ of SO_4^{2-}, and 614.15 $mg{\cdot}L^{-1}$ of Cl^- based on the composition of the effluent from a printed circuit electronic factory. The pH was adjusted by adding HNO_3 0.1 M and NaOH 0.1 M (Panreac, Barcelona, Spain) and the temperature was maintained constant at 22 °C ± 1 °C.

The aqueous concentrations of Cu(II), Pb(II), Cd(II), Cr(VI), and Ni (II) were measured at both the influent and the effluent of the fixed-bed adsorption column by inductively coupled plasma atomic emission spectroscopy analysis (ICP-AES, Agilent 4200 MP-AES, USA). Calibration curves were built by analysing standard solutions prepared by diluting certified standards of each metal at the same pH and the matrix media of the experimental mixtures. The certified standard solutions were acquired at a concentration of 1000 $mg{\cdot}L^{-1}$ (SPEX CertiPrep, United Kingdom and Merck Mollet del Vallès, Spain).

2.4. Adsorption/desorption experiments

2.4.1. Batch adsorption

Batch adsorption experiments were only conducted in the case of Cu (II) given that the composition of the synthetic solution mimicking the effluent of a printed circuit electronic factory can affect the sorption capacity of pinecone shells. The adsorption isotherms by pinecone shells for Pb(II), Cu(II), Cd(II) and Cr(VI) in aqueous media were characterized in a previous study (Amar et al., 2021).

Weighed amounts of the biosorbent were added to 20 mL of the synthetic electronic factory effluent, resulting in biosorbent concentrations ranging from 2 $g{\cdot}L^{-1}$ to 12 $g{\cdot}L^{-1}$. The mixtures were then agitated in a rotary mixer for 2 h to reach equilibrium, and the adsorption percentage was calculated by determining the difference between the initial Cu concentration and the concentration at equilibrium using ICP-OES. After the adsorption process, the samples were filtered, and the desorption of Cu(II) was carried out using 20 mL of 1.0 M of hydrochloric acid (HCl) for 2 h.

2.4.2. Fixed bed column

Fixed-bed column adsorption experiments were carried out to determine the performance of milled pinecone shells towards metal removal from both single metal and multi-component tests. A lab-scale glass column (12 mm of diameter and 200 mm length) with a fritted glass at the bottom was packed up to a pre-established height ranging from 5 to 10 mm corresponding to a known amount of adsorbent that was accurately weighed. The packing density was controlled by the height of a given weight of biosorbent in the column.

The influent metal or multimetal solutions at different concentrations and adjusted pH value were passed through the column at a constant flow in a range from 1.4 to 3.0 $mL{\cdot}min^{-1}$ controlled and impulsed by a peristaltic pump (Minipuls 3, Gilson Incorporated, Middleton, WI, USA). Careful consideration was given to preventing excessive pressure drop and ensuring uniform flow distribution while avoiding channelling within the column.

Samples of the solution were collected at prespecified times until the concentration of the exit C_t is equal to that of the entry C_i (saturation). Once the metals were adsorbed in the fixed-bed column, desorption experiments were performed to desorb the metal ions retained onto the adsorbent using 1.0 M HCl as the eluant.

The amounts of metal adsorbed at the different prespecified times were calculated by the difference between the initial concentration of the metal and the concentration in the sample collected at the same prespecified time. The dynamic response of the adsorption column was determined by the breakthrough time (t_b), corresponding to the moment at which the metal concentration of adsorbate reaches 5 % of the feed concentration ($C/C_i = 0.05$), and the shape of the breakthrough curve. The exhaustion time (t_s) was set as the time when the effluent concentration exceeded the 95 % of the initial concentration (Vera et al., 2018).

2.5. Mathematical modelling

The accurate fitting of experimental breakthrough curves is of paramount importance in understanding the adsorption kinetics and determining the model parameters. In this study, the implemented solution method is the outlined in (Aguareles et al., 2023; Myers et al., 2023) which treats the contaminant concentration as a travelling wave, coupled to a Sips model (Sips, 1948) to describe the rate of adsorption. As will be demonstrated this approach leads to an accurate fit of the experimental data, so providing insights into the adsorption mechanism in a fixed-bed column.

The Sips model may be written as

$$\frac{\partial q}{\partial t} = k_a C^m (q_m - q)^n - k_d q^n \tag{1}$$

where q_m is the maximum possible adsorbed fraction, k_a, k_d represent the adsorption and desorption coefficients. In a single stage reaction the exponents m, n are the stoichiometric coefficients. The equilibrium (saturation) adsorbed fraction, where adsorption balances desorption, may be found by setting the time derivative in (1) to zero and rearranging

$$q_e = \frac{q_m}{1 + \left(k_d / \left(k_a\, C_e^m\right)\right)^{1/n}} \tag{2}$$

where subscript e refers to the equilibrium value. For column adsorption the equilibrium concentration is the inlet value, $C_e = C_i$. Aguareles et al.

(2023) provide a list of solutions for the coupled system of contaminant flow with a Sips sink, defining the breakthrough shape against time for a range of m, n values, for the case $m = 1, n = 2$ the solution is given in implicit form. In Eq. (3) we present a rearranged and simplified form of their solution.

$$t = t_{1/2} + \frac{q_m}{k_a\, C_i\, (a^2 - 1)} \left[a^2 ln(C/(C_i - C)) + ln\left(\frac{a^2 C_i - C}{C(2a^2 - 1)} \right) \right] \quad (3)$$

where $a = q_m/q_e > 1$. In Section 3 we will investigate how Eq. (3) and other solutions taken from (Aguareles et al., 2023) match experimental data.

3. Results and discussion

3.1. Modelling of metal adsorption in fixed-bed column

3.1.1. Cu(II) adsorption

The copper content in industrial effluents, such as from a printed circuit electronic factory, can vary from 80 to 500 mg·L^{-1}, which does not meet regulatory standard of 3 mg.L^{-1} (BOE-A-1993-31103). To assess the practical applicability of the fixed-bed system using pinecone shells as an adsorbent, a synthetic solution was prepared to simulate the composition of these effluents, comprising various components, including 123.94 mg·L^{-1} of Cu(II), 11.28 mg·L^{-1} of NO_3^- 2.68 mg·L^{-1} of NO_2^-, 418.83 mg·L^{-1} of SO_4^{2-}, and 614.15 mg·L^{-1} of Cl^- at pH 5.5.

Batch experiments were conducted to estimate the optimal amount of adsorbent required to achieve adsorption efficiencies exceeding 90 %. Various biosorbent concentrations, ranging from 2 g·L^{-1} to 12.5 g·L^{-1} were tested in batch experiments. The maximum Cu(II) uptake was 16.7 mg·g^{-1}, observed when using an adsorbent dosage of 5 g·L^{-1}, whereas the maximum removal efficiency, 92.14 %, was achieved with the maximum applied adsorbent dosage. Table SI-1 presents the results expressed as removal efficiency, and Cu(II) uptake in equilibrium for each experiment, where each result is an average of three experiments using the same initial conditions. The difference is explained by taking into consideration the balance between the available adsorption sites on the pinecone shells surface and the concentration of Cu(II) in the solution. At low dosages, there were not enough active adsorption sites on the adsorbent surface to efficiently remove all the Cu(II) present in the solution, resulting in a lower removal percentage. On the other hand, at high dosages, an excess of the adsorbent leads to the non-saturation of adsorption sites.

To recover the adsorbed copper from the pinecone shells, an elution process was conducted using 20 mL of a 1.0 M HCl solution. The elution process achieved an efficiency of 70 % after 2 h, indicating that a significant portion of the adsorbed Cu(II) was successfully desorbed from the adsorbent surface.

Fig. 1 shows the isotherm data for the seven Cu(II) experiments. Although this set deals with the effect of varying adsorbent dosage, we assume this does not affect the adsorption capacity. The ratio of adsorption to desorption $K = k_a/k_d$, and saturation adsorption q_m may be calculated through a fit of the isotherm data using the formula

$$q_e = \frac{q_m K^{1/n} C_e^{m/n}}{1 + K^{1/n} C_e^{m/n}} \rightarrow y = \frac{Ax^b}{1 + Bx^b} \quad (4)$$

where $A = q_m K^{1/n}$, $B = K^{1/n}$ and $b = m/n$.

The results for each m, n pair can be found in Table SI-2. The fit of the models to the experimental data is poor, with R^2 values around 0.6 and no clear best m, n combination is seen in the isotherm data. This is likely attributed to the presence of relatively high concentrations of other anions in the solution, which can influence the formation of $CuCl^+$ and $CuCl_2^-$ complexes affecting Cu(II) adsorption.

Fixed-bed adsorption tests were conducted in column filled up to 10 mm and 20 mm, corresponding to 330 mg and 660 mg of adsorbent, respectively. The influent solution had a Cu(II) concentration of 120 mg·L^{-1}, containing NO_3^-, NO_2^-, SO_4^{2-}, and Cl^- at the specified concentrations in Section 2, with the pH adjusted to 5.5. The flowrate was set at 2.0 mL·min^{-1}.

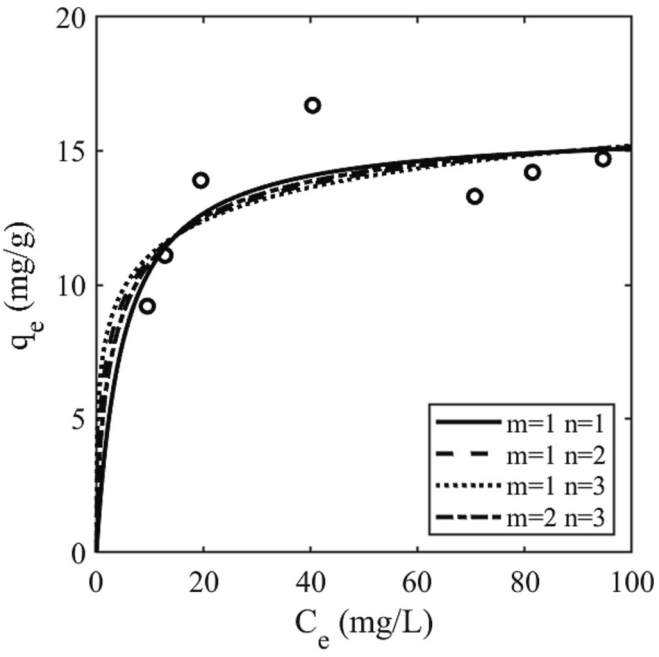

Fig. 1. Cu(II) equilibrium adsorption curves obtained in batch testing. Curves were fitted using Sips isotherm, Eq. (4), for four combinations of m and n. Data is provided in Table SI-1.

The breakthrough data generated from these experiments is presented in Fig. 2A and B as well as the analytical curves for four different m, n pairs (Aguareles et al., 2023). Note that the q_m obtained from the batch experiments usually differs from the one obtained in column experiments, while the equilibrium constant, K, should be the same for both forms of experiment. Consequently, we obtain the q_m value from the Sips isotherm with K taken from the batch results and q_e from the experiments. In this way there remains a single fitting parameter k_a to match the analytical curves to the breakthrough data.

The fitting was achieved using the Matlab function *lsqcurvefit* which minimises the least squares error. In Myers et al. (2023) it is pointed out that a good fit cannot be judged solely by the coefficient of determination, R^2, since even a poor fitting can result in a high value. It is necessary to also apply further criteria, such as the Sum of Squares Error (SSE). A high R^2 combined with a relatively low SSE will ensure a more robust fitting.

In both graphs of Fig. 2, it is apparent that the m = 1, $n = 2$ and m = 1, $n = 3$ solutions provide a good fit while the other two curves do not. The goodness of fit for all curves is provided in Table SI-3. Since both m = 1, n = 2 and m = 1, n = 3 results lead to a similar level of accuracy, we choose between models by assuming that the kinetics are related to the valence of the ion and so prefer the m = 1, n = 2 option described by Eq. (3).

The resultant values for q_m, k_a, calculated with m = 1, n = 2 are presented in Table 2. The goodness of fit is confirmed by the high R^2 and low SSE values. The isotherm indicated $k_d/k_a = 0.2162$ L g·mg^2, which permits the calculation of k_d if required. The calculated values should be independent of bed height, here we see an approximately 14 % variation in q_m and 26 % in k_a. The variations are too high to be accounted for through the 8 % change in inlet concentration. By defining column exhaustion as the time when the outlet concentration was 95 % of the inlet value, the measured q_e values were almost constant (11.1 mg·g^{-1} for the 10 mm bed and 11.2 mg·g^{-1} for the 20 mm bed) suggesting that the calculated variation in q_m arises due to isotherm values.

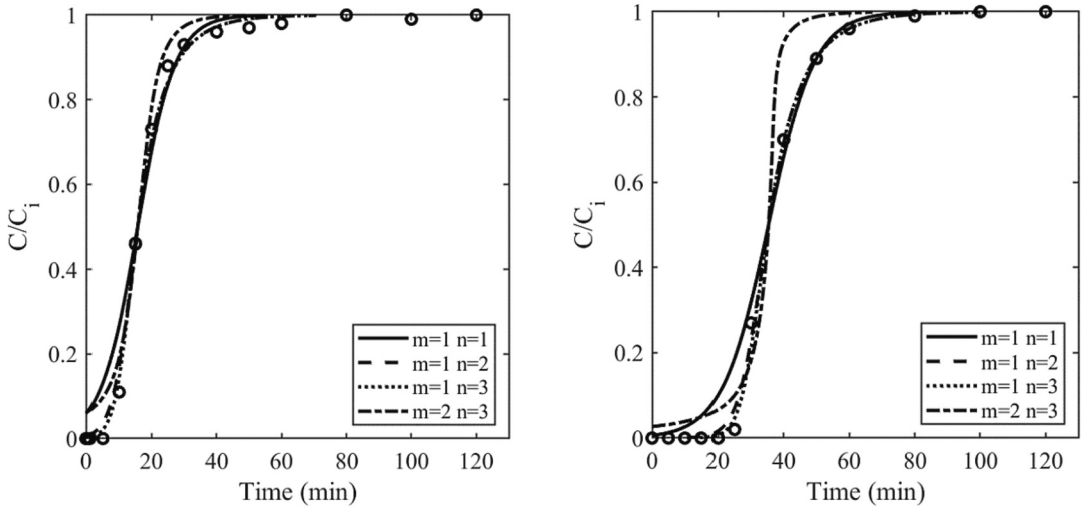

Fig. 2. Cu(II) adsorption breakthrough curves obtained at different bed heights: A) 10 mm and B) 20 mm. Circles represent experimental data points, curves represent the analytical solutions of Aguareles et al. (2023) for four different m, n pairs.

Table 2
Adsorption coefficient and goodness of the fit obtained from the fitting of the experimental breakthrough data points of Cu(II) adsorption using Eq. (3) (corresponding to m = 1, $n = 2$).

Experimental values						Fitted	Goodness of fit	
Initial conc. [mg·L^{-1}]	Flow rate [mL·min^{-1}]	Bed height [mm]	Initial mass [mg]	Adsorbed fraction q_e [mg·g^{-1}]	q_m [mg·g^{-1}]	k_a [L·g·mg^{-2}·s^{-1}] [x10^{-7}]	R^2	SSE
120.9	2.0	10	330	11.1	13.3	3.10	0.9964	0.0086
111.0	2.0	20	660	11.2	15.4	2.27	0.9983	0.0045

3.1.2. Pb(II) adsorption

Column experiments were carried out for Pb(II) adsorption with flow rates ranging from 1.4 to 3.0 mL·min^{-1}, and inlet concentrations between 9.8 and 96.7 mg·L^{-1}, as summarized in Table 3. We estimated K from the equilibrium data of the 7 mm bed length, flow rate 2.65 mL·min^{-1} experiments and assumed this held for the remaining experimental conditions. Then q_m was calculated for each case using the Sips isotherm expression with the experimental value of q_e. We once again examine different m, n values when dealing with breakthrough data, and the goodness of the fit for different m,n is shown in Table SI-4.

Fig. 3 presents the comparison of four different breakthrough curves with the experimental data obtained in column adsorption of Pb(II) using a bed height of 7 mm, a flow rate 2.65 mL·min^{-1} and different inlet concentrations. The value of q_m obtained from the isotherm study for each m, n combination has been used (Table SI-4), thus only k_a is fitted. Table SI-5 shows the goodness of fit of all four experiments with 7 mm bed and flow rate 2.65 mL·min^{-1}. At the lowest inlet concentration all three curves with m = 1 provide a good fit, but as the concentration increases it is clear that m = 1, $n = 2$ and m = 1, $n = 3$ solutions are the most accurate. Fig. 3B shows that m = 1, n = 3 does not accurately capture the initial breakthrough. For this reason, and due to the valence, we once again prefer the m = 1 n = 2 model, Eq. (3), to describe the breakthrough of Pb(II) onto pinecone shell in the fixed-bed column system. In fact, the metrics, R^2 and SSE, indicated the same combination of m, nas optimal across all the experimental data sets, further reinforcing the suitability of Eq. (3) to fit the experimental data.

The goodness of fit for the case m = 1, n = 2 is shown in Table 3. With a fixed flowrate we expect both k_a, q_m to remain constant. For the first three rows both remain relatively constant, within experimental error. The fourth row shows a jump in values, as well as a much worse fit (as seen from the R^2 and SSE values). The low inlet concentration in this case may result in a different adsorption reaction/isotherm such that Eq. (3) may not be the best model here. In Rows 5–7, the effect of varying bed length is demonstrated. It is observed that bed height has no

Table 3
Experimental conditions and calculated parameters for Pb(II) column adsorption.

Experimental values						Fitted	Goodness of fit	
Conc. [mg·L^{-1}]	Flow rate [mL·min^{-1}]	Bed height [mm]	Initial mass [mg]	Adsorbed fraction q_e [mg·g^{-1}]	q_m [mg·g^{-1}]	k_a [L·g·mg^{-2}·s^{-1}] (x10^{-7})	R^2	SSE
96.7	2.65	7	220	55.57	62.28	3.13	0.9976	0.0024
69.3	2.65	7	220	49.76		3.84	0.9903	0.0211
46.8	2.65	7	220	52.25		3.87	0.9879	0.0245
9.8	2.65	7	220	17.50		4.48	0.9787	0.0346
43.0	2.20	10	330	38.44	52.40	4.02	0.9770	0.0575
46.5	2.20	7	220	42.63		4.21	0.9928	0.0193
48.5	2.20	5	150	49.89		7.78	0.9979	0.0052
46.5	3.00	7	220	44.11	67.06[a]	2.31	0.9755	0.0452
46.7	2.20	7	220	40.26	52.40	3.58	0.9949	0.0097
46.5	1.40	7	220	26.16	31.99	9.43	0.9911	0.0190

[a] Extrapolated using the q_m values obtained at 1.4, 2.2 and 2.6 mL·min^{-1}.

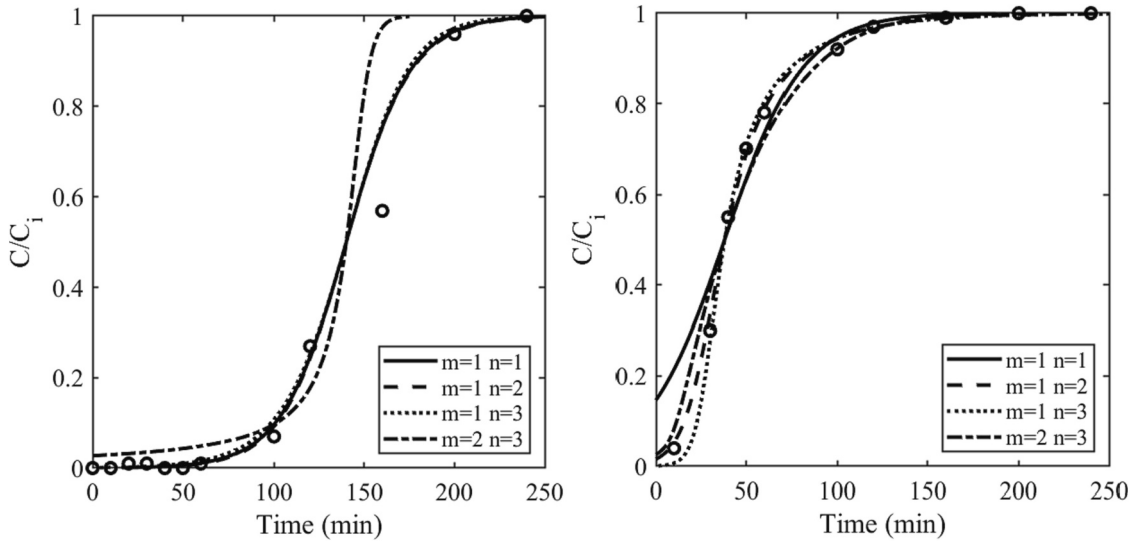

Fig. 3. Pb(II) adsorption breakthrough curves obtained at A) C_i 9.8 mg·L^{-1}; B) C_i 96.7 mg·L^{-1}. Data points shown as circles, analytical curves using the analytical solutions of Aguareles et al. (2023) for diverse m and n shown as lines. pH 5.6, bed height 7 mm, flowrate 2.65 mL·min^{-1}.

noticeable effect on k_a between 7 and 10 mm, but that it is almost doubled for 5 mm. This difference in the 5 mm results is most likely caused by the breakdown of the solution method employed by Aguareles et al. Their results are based on a travelling wave assumption, that the concentration profile travels in a self-similar form along the column. This places restrictions on the time when it may be applied, since it must evolve from the initial shape to the travelling wave. Referring to Fig. 4, it is observed that the breakthrough time is very close to zero, suggesting that the travelling wave has not yet formed. In which case the estimate for k_a will be incorrect. For the final three rows, the effect of changing the flow rate is presented. The maximum adsorbed mass remains relatively constant but the adsorption coefficient k_a shows an almost linear decrease with flow rate.

Fig. 4 shows the fitting of Eq. (3) to a variety of data, with three bed heights and flow rates. The modelling results provided valuable insights into the adsorption mechanism. The adsorption kinetics are first order with respect to Pb(II) (variable C), and second order with respect to the active adsorption sites on the adsorbent surface (q_m-q). This suggests that each Pb(II) ion requires two active surface sites to get adsorbed. Most R^2 values are above 0.99 whereas the maximum sum of squared errors is 0.0575, indicating a strong correlation between the model and the experimental results.

3.2. Competitive multimetal adsorption in fixed-bed column

The good metal adsorption performance of milled pinecone shells observed in single-metal solutions has prompted further exploration of its potential in removing toxic metals from multicomponent water solutions. In this section, the adsorption behaviour of ternary metal solutions containing Cu(II) and Cd(II) in competition with Pb(II) using a fixed-bed column set-up was investigated. The influent concentrations of each metal were varied from 25 mg·L^{-1} to 100 mg·L^{-1}, and the dynamic adsorption experiments were conducted with a fixed-bed height of 10 mm with an influent flow rate of 2.2 mL· min^{-1}.

Fig. 5 displays the breakthrough curves obtained from the dynamic adsorption experiments. At each influent metal concentration, Pb(II)

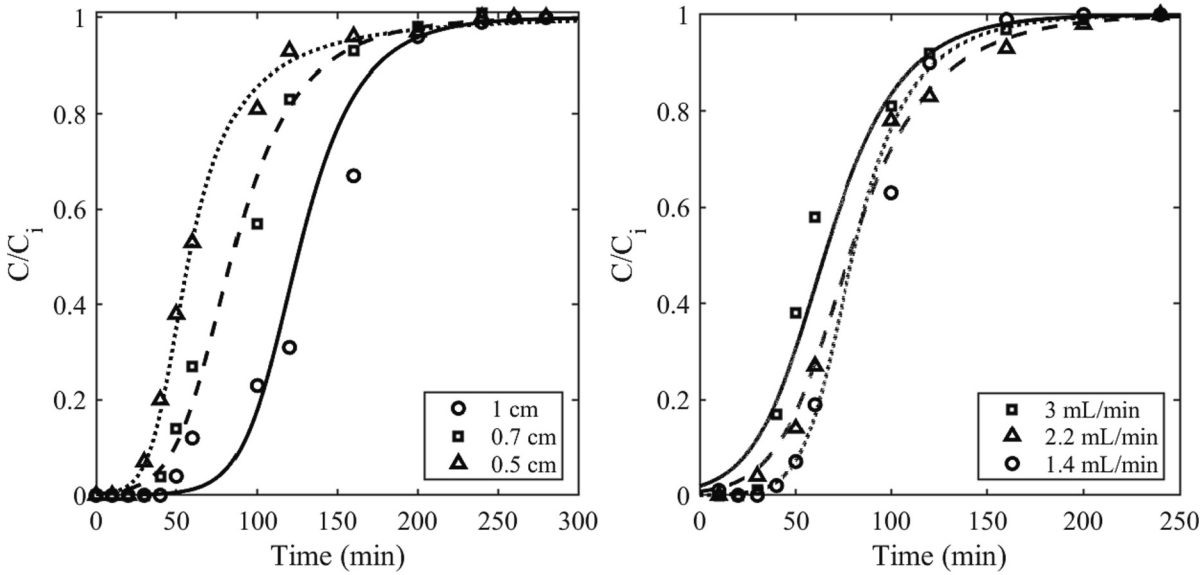

Fig. 4. Pb(II) adsorption breakthrough curves obtained at A) different bed heights (C_i 43.0, 46.5 and 48.5 mg·L^{-1}, flowrate 2.2 mL·min^{-1}), B) different flowrates (C_i 46.5, 46.75 and 46.5 mg·L^{-1}, bed height 7 mm). Data points shown as circles, triangles and squares, fitting is via Eq. (3).

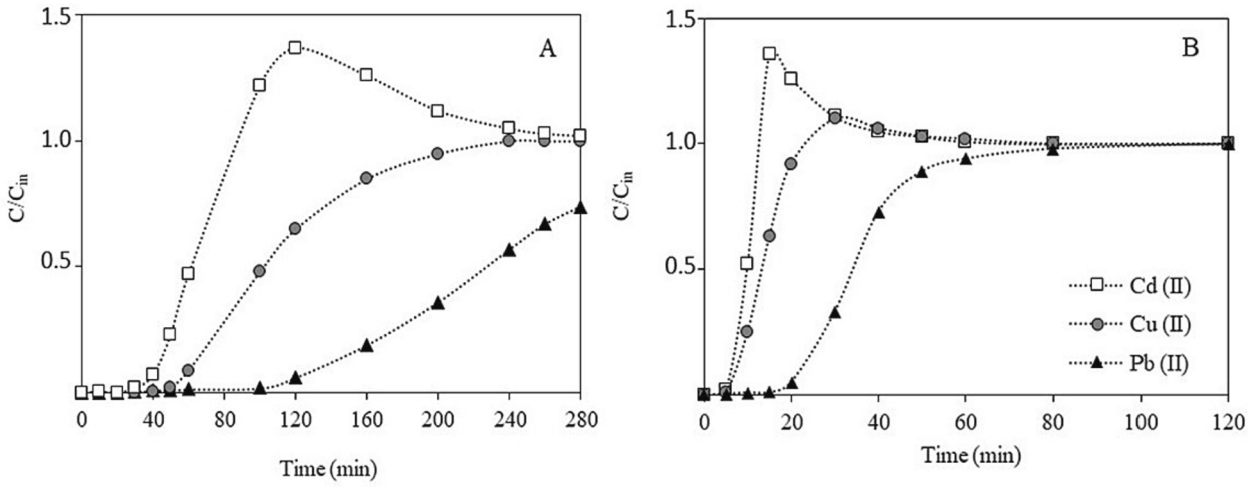

Fig. 5. Competitive adsorption breakthrough curves of Cu (II), Pb(II) and Cd(II) obtained at different inlet concentrations: A) 25 mg·L^{-1}, B) 100 mg·L^{-1}. Bed height 10 mm, pH 5.6, flowrate 2.2 mL·min^{-1}.

exhibited the highest affinity for the pinecone shells adsorbent, as evidenced by the longest breakthrough times. This observation aligns with the results from the single-component adsorption tests, where Pb(II) demonstrated a higher adsorption capacity compared to Cu(II) (Tables 2, 3).

The competitive nature of adsorption among the different metal ions led to a displacement of the weakest adsorbed species, resulting in a roll-up effect where the previously adsorbed ions are desorbed, and the concentration at the outlet of the column is higher compared to the influent concentration ($C/C_{in} > 1$). In all cases, Cd(II) was the weakest adsorbed ion, resulting in pronounced desorption that led to Cd(II) uptakes ranging between 2.5 and 5 mg·g^{-1} for both the tests at 25 and 100 mg·L^{-1} influent concentrations. This behaviour was also observed when citrus peels were utilized for dynamic biosorption of Pb, Cd, and Zn from mono- and bi-component solutions in fixed-bed columns (Chatterjee and Schiewer, 2014).

The tests with 25 mg·L^{-1} influent concentration ran for 280 min, which did not allow for bed exhaustion. In contrast, the tests depicted in Fig. 4B, conducted with an influent metal's concentration of 100 mg·g^{-1}, reached bed exhaustion after 59 min. During these experiments, Cu(II) exhibited a slight roll-up effect, resulting in a final uptake of 7.6 mg·g^{-1}. However, the Pb(II) uptake was only 23.8 mg·g^{-1}, considerably lower than what would be expected based on to the single metal adsorption tests. Thus, the competition between the metals had a noticeable impact on the adsorption performance.

The preferential selectivity of Pb(II) over the other two metal ions, Cu(II) and Cd(II), can be attributed to key factors. Pb(II) exhibits a favourable hard-hard interaction with hard ligands, such as carboxyl and hydroxyl groups. This interaction is further enhanced by its smaller hydrated ion radius, lower hydrolysis constant, and a higher degree of covalent bonding character (Amar et al., 2021, 2020; Chatterjee and Schiewer, 2014).

The lower degree of hydration of Pb(II) results in fewer tightly-bound water molecules around the ion. This reduced hydration allows for greater accessibility to the surface of the adsorbent, thereby facilitating adsorption. Additionally, Pb(II) possesses a larger ionic radius compared to Cu(II) and Cd(II). This larger ionic radius enables Pb(II) to establish stronger bonds with the functional groups on the adsorbent's surface due to its size advantage (Finish et al., 2023).

Furthermore, Pb(II) exhibits a higher covalent index of in contrast to Cu(II) and Cd(II). This higher covalent index indicates a greater propensity to form covalent bonds with the functional groups on the adsorbent. As a result, Pb(II) forms more robust bonds with the adsorbent, further enhancing its selectivity and showing the affinity order (Pb (II) > Cu(II) > Cd(II)) previously observed when grape stalks waste were used for fixed-bed column multimetal adsorption modelling (Escudero et al., 2013).

3.3. Surface characterization of pristine and spent samples

The SEM micrograph of the pristine pinecone shells (shown in Supplementary information, Fig. SI-1A) revealed an irregular and uneven surface. Subsequent SEM images of the adsorbent after exposure to metal adsorption show noticeable modifications, including the accumulation of metals in the cracks and crevices of the adsorbent surface.

The EDS and EDX analyses (Fig. SI-1B) provide a valuable qualitative assessment of changes in elemental composition. Initially present elements, including Mg, K, and Ca on the pristine pinecone shell surface, exhibited variations depending on the sample surface analysed with weight percentages of ~0.15 % of Mg, ~0.7 % of Ca, and 0.3 % of K; their signal almost disappeared following the adsorption of Pb(II), Cu (II), and Cd(II). Notably, signals corresponding to Pb, Cu, and Cd with weight percentages of ~8 % of Cu, 20 % of Pb, and 0.5 % of Cd, are detected in exhausted samples from the ternary mixture tests, suggesting the effective adsorption of these metals by the pinecone shells and indicating the greater affinity of this biosorbent for Pb, followed by Cu and Cd.

To understand the structural changes in milled pinecone before and after metal adsorption, FTIR and XRD analyses were conducted. The FTIR spectrum of adsorbent surface, presented in Fig. 6, revealed characteristic bands corresponding to various functional groups found in lignocellulosic substrates.

The broad band observed at 3268 cm^{-1} indicated the presence of hydroxyl groups (O—H stretching vibration) in the cellulose moiety. The peak at 2929 cm^{-1} indicated the stretching vibration of aliphatic C—H groups, while the peak at 1611 cm^{-1} denoted the stretching vibration of C═O in carboxyl groups. Additionally, the peak at 1030 cm^{-1} represented the stretching vibration of C—O in primary alcohol groups. These observed peaks and bands are consistent with the reported spectra of lignocellulosic materials (Ravat et al., 2000).

Upon metal adsorption, noticeable changes were observed in these peaks, including band shifts and a decrease in intensity. These changes suggest that the hydroxyl and carboxyl groups are involved in the adsorption of metals through processes such as ion exchange and surface complexation (Ravat et al., 2000).

The alterations in the FT-IR spectrum further confirm the interaction between pinecone shells functional groups and the metal ions during the adsorption process. The good fit achieved for the adsorption model of Pb

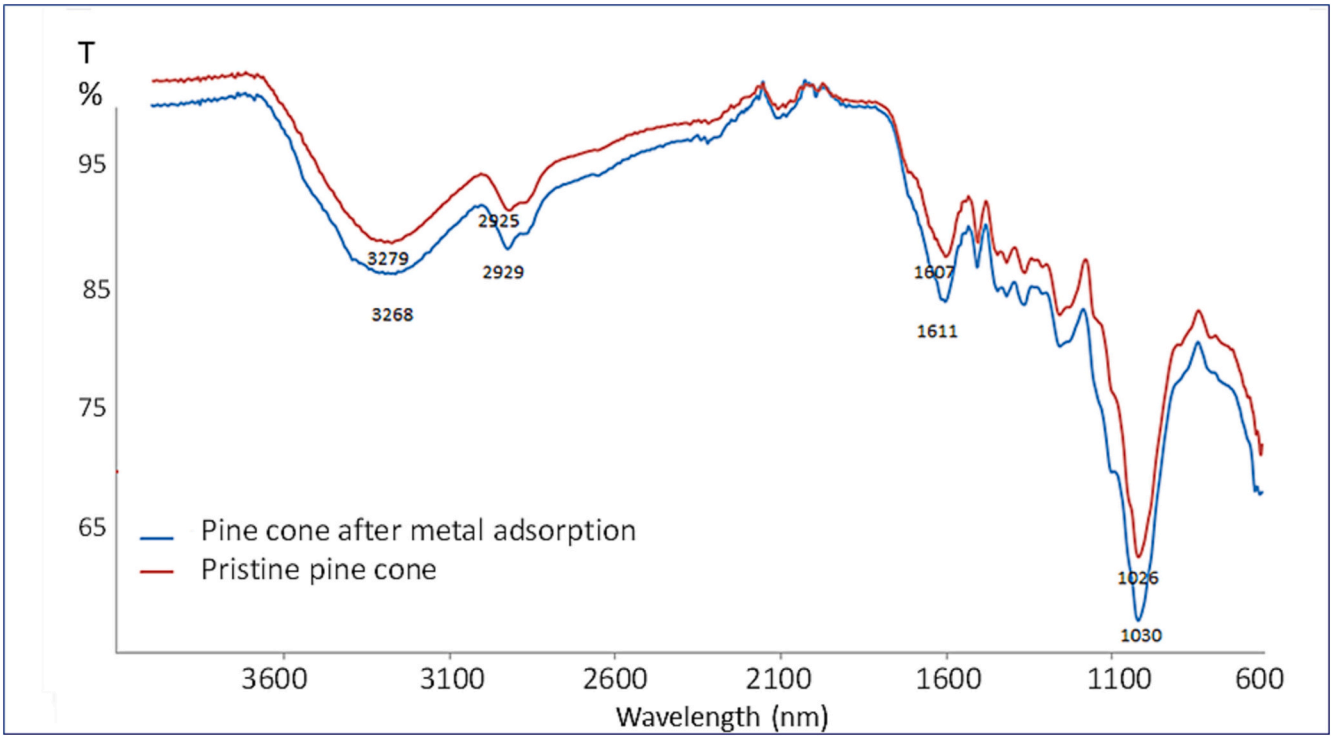

Fig. 6. FT-IR of pinecone shells before adsorption (blue) and after adsorption (red) of Cu(II), Pb(II), and Cd(II).

(II) with m = 1 and $n = 2$ (Table 3) agrees with a surface complexation mechanism, based on the association of Pb(II) with the carboxyl and OH groups of the surface rather than on an ion-exchange mechanism.

X-ray diffraction (XRD) analysis was used to examine the crystalline nature of milled pinecone shells before and after metal adsorption (Fig. 7). The broad peak observed at 2θ ranging from 11° to 34° is characteristic of the amorphous phase, encompassing components present in biosorbents such as lignin, hemicellulose, and amorphous cellulose (Wang et al., 2022). Additionally, the diffractogram exhibited distinct peaks at 2θ = 16°, 22°, and 34°, corresponding to crystalline planes of the cellulose structure, with a calculated crystallinity index of 18.89 % (Kumar et al., 2021).

Upon adsorption of Pb(II)/Cu(II)/Cd(II) ions, changes were observed in the XRD diffractograms. These peaks became weaker and broader, indicating a reduction in pinecone shells crystallinity. This suggests the conversion of crystalline regions into disoriented amorphous regions after binding with Pb(II)/Cu(II)/Cd(II) ions. The disruption of hydrogen bonds maintaining ordered crystalline regions is likely responsible for this observed decrease in crystallinity (Wang et al., 2022).

These characterizations provide valuable insights into the structural

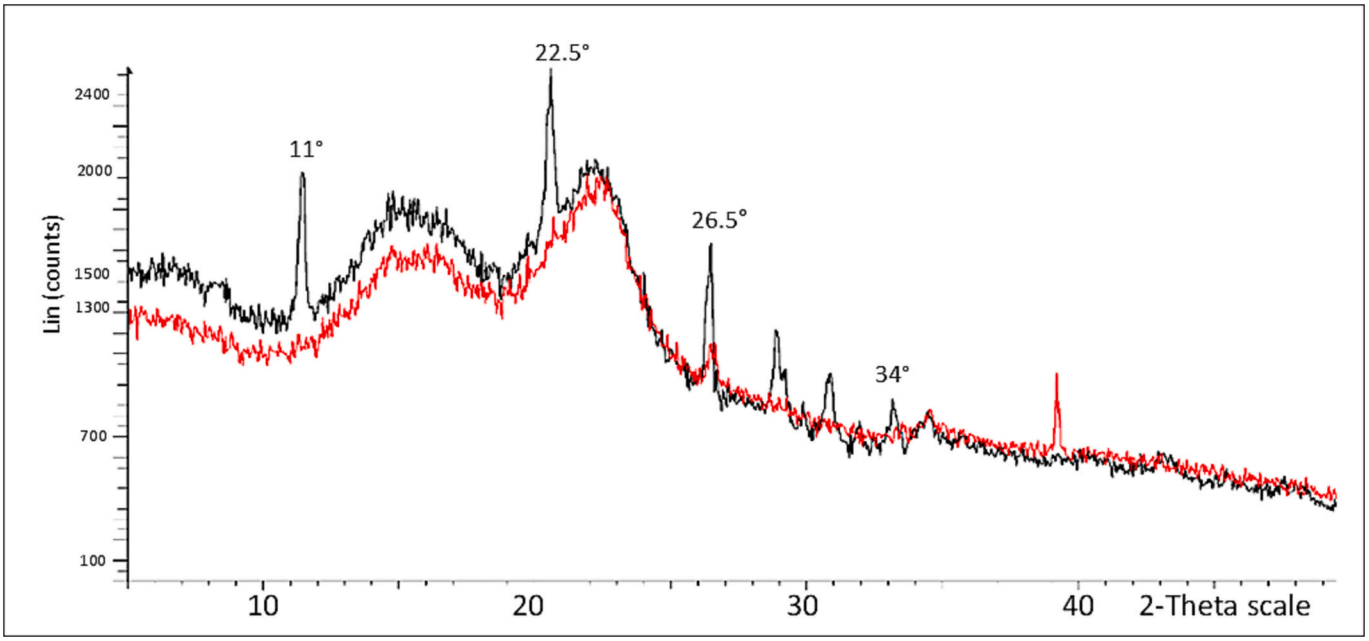

Fig. 7. XRD diffractograms of pine cone (black) and pine cone containing Cu(II), Cd(II), and Pb(II) (red).

changes occurring in the surface during metal adsorption. The alterations observed in FTIR and XRD analyses confirm the active involvement of functional groups on the surface of the pinecone shells, supporting its capacity to selectively bind with metal ions.

3.4. Interaction of heavy metals with common water ions

To gain further insights into the adsorption behaviour of Pb(II), Cu (II), and Cd(II) in the presence of ions commonly found in water, a series of competitive fixed-bed dynamic adsorption tests was conducted. The effect of soft cations such as K^+, Ca^{2+}, Na^+, and Mg^{2+} on heavy metal adsorption can be attributed to both cation exchange and mineral precipitation (Deng et al., 2019). Thus, calcium was selected as the representative soft divalent cation due to its prevalence in water and its potential to compete with toxic metal ions for the adsorbent surface, particularly when the interaction between the metal ions and the surface functional groups involves an ion-exchange mechanism (Agarwal et al., 2020).

The breakthrough curves obtained for each metal at an influent concentration of 50 mg·L^{-1} in the presence of 100 mg·L^{-1} Ca(II) are shown in Fig. 8. It was observed that Ca(II) was not adsorbed in the presence of the other metal ions. Furthermore, the higher concentration of Ca(II) in solution did not hamper the adsorption performance towards Cu(II) and Pb(II), presenting uptakes at bed exhaustion of 9.9 and 20.9 mg·g^{-1}, respectively, and 4.5 mg·g^{-1} for Cd(II).

These findings suggest that the adsorption mechanism for Pb(II) and Cu(II) ions is likely to involve surface complexation facilitated by the presence of hydroxyl and carboxyl functional groups on the pinecone shells surface, in accordance with the modelling results (m = 1, n = 2) obtained for Cu(II) and Pb(II) adsorption (Section 3.1).

These functional groups act as ligands, forming complexes with the metal ions, rather than relying solely on electrostatic interactions between the metal ions and the negatively charged sites of surface that may result in deprotonation (Amar et al., 2021).

The competitive adsorption results underscore the importance of understanding the interactions between different metal ions and divalent cations such as Ca(II) in complex water matrices. Depending on the adsorption mechanism, the presence of Ca(II) can significantly influence the overall adsorption capacity of the biosorbent for toxic metal ions (Chatterjee and Schiewer, 2014). However, since metal adsorption occur through surface complexation, Ca(II) ions does not affect the removal efficiency, showing that pinecone shell is an effective biosorbent for wastewater treatment in environments where divalent cations are abundant (Stala et al., 2022, 2021).

3.5. Competitive adsorption and desorption processes

The efficient removal of heavy metal ions from industrial wastewater is of utmost importance to mitigate environmental pollution and ensure compliance with regulatory standards. Electroplating industry effluents represent an example that is particularly challenging due to the presence of multiple metal ions at varying concentrations as well as other toxic components as cyanide, organic solvents, and high content in organic matter and suspended solids (Rajoria et al., 2022). In this section, the adsorption performance of milled pinecone shell was investigated for the simultaneous removal of 20 mg·L^{-1} of Cu(II), 100 mg·L^{-1} of Ni(II), and 30 mg·L^{-1} of Cr(VI) at pH = 4.4 from a synthetic aqueous solution mimicking the metal composition and pH of an electroplating effluent (Singh and Ram, 2016).

Fixed-bed column experiments were conducted to evaluate the adsorption breakthrough curves of these three metal ions under the specified conditions. As shown in Fig. 9A, the breakthrough curves revealed distinct adsorption behaviours. Cr(VI), which was successfully removed at pH 2 in preliminary batch tests (Amar et al., 2021) exhibited the fastest breakthrough in competitive adsorption at pH 4.4, indicating its weak affinity for the biosorbent at mild conditions, with an adsorption capacities at bed exhaustion of 1.51 mg·g^{-1}. Ni(II) followed with a relatively rapid breakthrough at 30 min, considering that the influent concentration of this metal was the highest. The Cu(II) breakthrough caused a displacement of the preadsorbed Ni(II), resulting in the so-called roll-up effect, suggesting weaker adsorption affinity for Ni(II).

The adsorption capacities at bed exhaustion for Cu(II) and Ni(II)

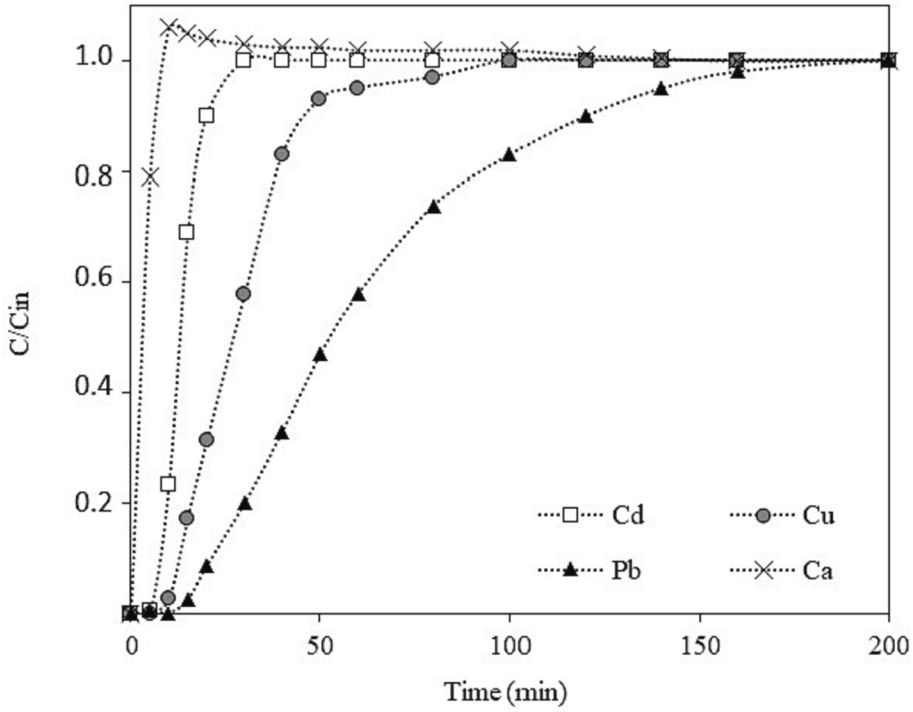

Fig. 8. Experimental breakthrough curves of a multimetal solution containing 50 mg·L^{-1} of Cd(II), Cu(II), Pb(II), and 100 mg·L^{-1} of Ca (II), pH 5.6, flow rate 2.2 mL·min^{-1} and bed height 10 mm (n = 3).

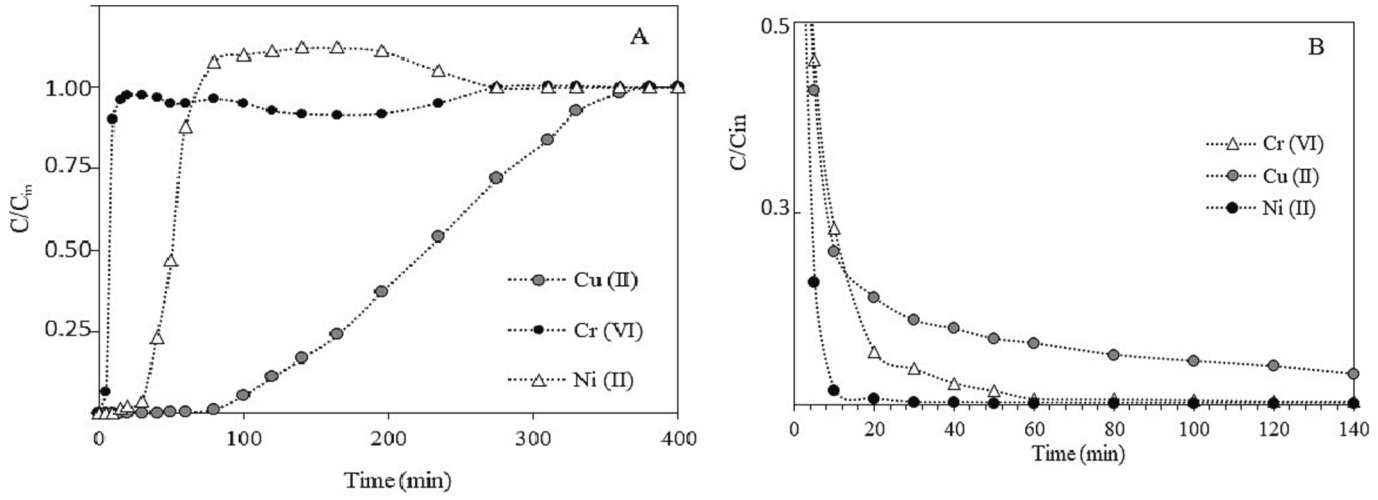

Fig. 9. Experimental breakthrough curves obtained at bed height 20 mm for A) adsorption - flow rate 2.2 mL·min^{-1}, influent concentrations of 20 mg·L^{-1} Cu(II), 30 mg·L^{-1} Cr(VI) and 100 mg·L^{-1} Ni(II), pH 4.4; B) desorption – flow rate 1.2 mL min^{-1} using 1.0 M HCl.

were 10.34 and 13.41 mg·g^{-1}, respectively. In fact, most of the studied metal adsorbents have more affinity for Cu(II) except when nitrogen functional groups, such as amines and amides are present in adsorbent surface, together with carboxyl and hydroxyl groups (Geng et al., 2022; Liang et al., 2022). Also, cation exchange and precipitation were the preferred adsorption mechanisms identified for Ni(II) in biochar (Deng et al., 2019). Given that Ni(II) influent concentration was five times higher than that of Cu(II), and the Cu(II) uptake was not reduced compared to the single tests at the same range of concentration it may be concluded that the presence of Ni(II) did not hamper the removal of Cu (II).

The regeneration and reusability of adsorbents are crucial considerations for practical applications in wastewater treatment processes. To evaluate the feasibility of metal desorption of the milled pinecone shells adsorbent and recovering the adsorbed metal ions, regeneration studies were conducted using 1.0 M HCl as the desorbing agent using a flow rate of 1.2 mL min^{-1} in the fixed-bed column. One advantage of employing acidic treatment for regeneration of the biosorbent is that acid solutions are common waste from many industries and employing them can contribute to its valorisation. HCl as desorbing agent is reported to recover >90 % of metal ions, despite numerous studies have shown that it causes hydrolysis of the functional groups present in biomass (Islam et al., 2023; Reshmy et al., 2022).

Fig. 9B illustrates the desorption curves obtained in 140 min operation. The recovery percentages after this period of time corresponded to 7.5 % for Cu(II), 33.6 % for Cr(VI) and 11.1 % for Ni(II). The recovery percentage for Cu(II) is very low in comparison with that obtained in the batch experiments (>70 % after 2 h, Section 3.1.1) and can be explained by the low contact time between the eluting solution and the adsorbent in the fixed-bed column despite the flow in the desorption test was reduced to 1.2 mL.min^{-1}. However, taking into consideration that pinecone biomass has a low cost and that biomass is a renewable resource of energy, destructive recovery by pyrolysis of the adsorbed metals from pinecone would be economically feasible (Martín-Lara et al., 2016b).

Overall, the findings of this study have practical significance and direct implications for environmental remediation strategies and sustainable wastewater treatment. The demonstrated effectiveness of milled pinecone shells as a biosorbent for heavy metal removal, particularly Cu(II) and Pb(II), underscores its potential application in the development of cost-effective and environmentally friendly water treatment technologies. The versatility of pinecone shells, as is seen by their consistent performance across various conditions, highlights their suitability for addressing heavy metal contamination in diverse industrial effluents. However, challenges may arise in scaling up the application of pinecone shells to larger treatment facilities, and further research is needed to explore the economic feasibility, long-term efficacy, and potential environmental impacts of deploying this biosorbent on an industrial scale.

4. Conclusions

The influence of various parameters, including initial adsorbate concentration, bed height, and flow rate, on the removal efficiency of Pb (II) by milled pinecone shell has been thoroughly investigated. The experimental data for Pb(II) and Cu(II) removal yielded adsorption capacities of 65 and 11 mg·g^{-1}, respectively, at influent concentrations over 100 mg·L^{-1} under the experimental conditions tested. Modelling was performed by considering a coupled system of metal ion flow with the Sips isotherm. The model with m = 1, $n = 2$ resulted in the strongest correlation with the experimental results and suggested that each Cu(II) and Pb(II) requires two active surface sites to be adsorbed. These results agree with a sorption mechanism based on surface complexation of the metal ions facilitated by the presence of hydroxyl and carboxyl functional groups on the pinecone shells surface.

In competitive adsorption experiments using aqueous solutions containing equal concentrations (50 and 100 mg·L^{-1}) of Cu(II), Cd(II), and Pb(II), pinecone clearly had a greater affinity for Pb(II), which showed the longest exhaustion time in the fixed-bed column while Cu(II) exhibited a slight roll-up effect, resulting in a final uptake of 7.6 mg·g^{-1}. However, the Pb(II) uptake was only 23.8 mg·g^{-1}, considerably lower than what would be expected based on single metal adsorption tests, showing that the competition between the metals had a noticeable impact on the adsorption performance in dynamic conditions.

Additionally, the investigation of the adsorption behaviour in the presence of soft metal ions, such as Ca(II), demonstrated that the uptake of Pb(II), Cu(II), and Cd(II) by pinecone shells remained unaffected, supporting the notion that surface complexation was the dominant adsorption mechanism. This suggests the versatility and robustness of pinecone shells as an efficient biosorbent for the removal of heavy metal ions from wastewater.

The adsorption of Cu(II), Ni(II), and Cr(VI) from an aqueous solution mimicking the metal composition and pH of an electroplating effluent, resulted in adsorption capacities at bed exhaustion for Cu(II) and Ni(II) of 10.34 and 13.41 mg·g^{-1}, respectively, showing that the presence of Ni (II) did not hamper the removal of Cu(II) despite its concentration being five times higher. In contrast, Cr(VI) displayed poor adsorption, since the pH = 4.4 was not optimal for this metal: maximum sorption

capacities for Cr(VI) were obtained in batch experiments at pH < 3.

The subsequent desorption of metal ions from milled pinecone shells using a 1.0 M HCl solution yielded poor desorption percentages that followed the order: Cr(VI) > Ni(II) > Cu(II). The low recovery percentage obtained for Cu(II) denotes its strong adsorption by pinecones, confirming that surface complexation is the main adsorption mechanism.

Supplementary data to this article can be found online at https://doi.org/10.1016/j.scitotenv.2024.170398.

CRediT authorship contribution statement

Marwa Ben Amar: Writing – original draft, Validation, Resources, Conceptualization. **Maryam Mallek:** Writing – review & editing, Investigation, Data curation. **Abel Valverde:** Writing – original draft, Validation, Software, Formal analysis. **Hèctor Monclús:** Visualization, Funding acquisition, Data curation. **Timothy G. Myers:** Writing – review & editing, Methodology, Formal analysis, Data curation. **Victoria Salvadó:** Writing – review & editing, Supervision, Project administration, Funding acquisition, Conceptualization. **Alba Cabrera-Codony:** Writing – original draft, Visualization, Validation, Supervision.

Declaration of competing interest

The authors declare the following financial interests/personal relationships which may be considered as potential competing interests:

Hector Monclus reports financial support was provided by Ministerio de Ciencia, Innovación y Universidades. Abel Valverde reports financial support was provided by Spanish Ministry of Universities with European Union. Timothy G. Myers reports financial support was provided by Spanish Ministry of Science Technology and Innovations. Victoria Salvador reports financial support was provided by Horizon 2020 Framework Programme. Marwa Ben Amar reports financial support was provided by University of Sfax. Maryam Mallek reports financial support was provided by University of Sfax. Alba Cabrera-Codony reports financial support was provided by Spanish Ministry of Science and Innovation. If there are other authors, they declare that they have no known competing financial interests or personal relationships that could have appeared to influence the work reported in this paper.

Data availability

Data will be made available on request.

Acknowledgments

This study was financed by the research project PID2019-107033GB-C22 (AEI/FEDER/UE) of the "Agencia Española de Investigación" MINECO. M.B. Amar and M. Mallek acknowledge the financial support of the Faculty of Science (University of Sfax, Tunisia) and of the Environmental and Analytical Chemistry Research Group of the Department of Chemistry (University of Girona, Spain).

A. Cabrera-Codony and H. Monclús acknowledge Agencia Estatal de Investigación of the Spanish Ministry of Science, Innovation and Universities (MCIU) for partially funding this research through Juan de la Cierva (IJC2019-038874-I) and Ramon y Cajal (RYC2019-026434-I) Fellowships. LEQUIA has been recognized as a consolidated research group (Ref 2021 SGR1352) by the Catalan Ministry of Research and Universities.

A. Valverde acknowledges support from the Margarita Salas UPC postdoctoral grants funded by the Spanish Ministry of Universities with European Union funds – NextGenerationEU (UNI/551/2021 UP2021-034). This publication is part of the research projects PID2020-115023RB-I00 (funding A. Cabrera-Codony and T. Myers) financed by MCIN/AEI/10.13039/501100011033/ and by "ERDF A way of making Europe". T. Myers acknowledges the CERCA Programme of the Generalitat de Catalunya and also the Spanish State Research Agency, through the Severo Ochoa and Maria de Maeztu Program for Centres and Units of Excellence in R&D (CEX2020-001084-M). Open Access funding provided thanks to the CRUE-CSIC agreement with Elsevier.

References

Afroze, S., Sen, T.K., 2018. A review on heavy metal ions and dye adsorption from water by agricultural solid waste adsorbents. Water Air Soil Pollut. 229, 225. https://doi.org/10.1007/s11270-018-3869-z.

Agarwal, A., Upadhyay, U., Sreedhar, I., Singh, S.A., Patel, C.M., 2020. A review on valorization of biomass in heavy metal removal from wastewater. J. Water Process Eng. 38, 101602 https://doi.org/10.1016/j.jwpe.2020.101602.

Aguareles, M., Barrabés, E., Myers, T., Valverde, A., 2023. Mathematical analysis of a Sips-based model for column adsorption. Phys. D: Nonlinear Phenom. 448 https://doi.org/10.1016/j.physd.2023.133690.

Amar, M. Ben, Walha, K., Salvadó, V., 2020. Evaluation of olive stones for Cd(II), Cu(II), Pb(II) and Cr(VI) biosorption from aqueous solution: equilibrium and kinetics. Int. J. Environ. Res. 14, 193–204. https://doi.org/10.1007/s41742-020-00246-5.

Amar, M. Ben, Walha, K., Salvadó, V., 2021. Valorisation of pine cone as an efficient biosorbent for the removal of Pb(II), Cd(II), Cu(II), and Cr(VI). Adsorpt. Sci. Technol. 2021, 1–12. https://doi.org/10.1155/2021/6678530.

Blázquez, G., Martín-Lara, M.A., Dionisio-Ruiz, E., Tenorio, G., Calero, M., 2011. Evaluation and comparison of the biosorption process of copper ions onto olive stone and pine bark. J. Ind. Eng. Chem. 17, 824–833. https://doi.org/10.1016/j.jiec.2011.08.003.

BOE-A-1993-31103 Ley 10/1993, de 26 de octubre, sobre Vertidos Líquidos Industriales al Sistema Integral de Saneamiento. [WWW Document], n.d. URL https://www.boe.es/eli/es-md/l/1993/10/26/10 (accessed 1.9.24).

Cabrera-Codony, A., Ruiz, B., Gil, R.R., Popartan, L.A., Santos-Clotas, E., Martín, M.J., Fuente, E., 2021. From biocollagenic waste to efficient biogas purification: applying circular economy in the leather industry. Environ. Technol. Innov. https://doi.org/10.1016/j.eti.2020.101229.

Chatterjee, A., Schiewer, S., 2014. Effect of competing cations (Pb, Cd, Zn, and Ca) in fixed-bed column biosorption and desorption from citrus peels. Water Air Soil Pollut. 225, 1854. https://doi.org/10.1007/s11270-013-1854-0.

Chauhan, D., Sankararamakrishnan, N., 2011. Modeling and evaluation on removal of hexavalent chromium from aqueous systems using fixed bed column. J. Hazard. Mater. 185, 55–62. https://doi.org/10.1016/j.jhazmat.2010.08.120.

Davila-Guzman, N.E., Cerino-Córdova, F.J., Loredo-Cancino, M., Rangel-Mendez, J.R., Gómez-González, R., Soto-Regalado, E., 2016. Studies of adsorption of heavy metals onto spent coffee ground: equilibrium, regeneration, and dynamic performance in a fixed-bed column. Int. J. Chem. Eng. 2016, 1–11. https://doi.org/10.1155/2016/9413879.

Deng, Y., Huang, S., Laird, D.A., Wang, X., Meng, Z., 2019. Adsorption behaviour and mechanisms of cadmium and nickel on rice straw biochars in single- and binary-metal systems. Chemosphere 218, 308–318. https://doi.org/10.1016/J.CHEMOSPHERE.2018.11.081.

Escudero, C., Poch, J., Villaescusa, I., 2013. Modelling of breakthrough curves of single and binary mixtures of Cu(II), Cd(II), Ni(II) and Pb(II) sorption onto grape stalks waste. Chem. Eng. J. 217, 129–138. https://doi.org/10.1016/j.cej.2012.11.096.

Finish, N., Ramos, P., Borojovich, E.J.C., Zeiri, O., Amar, Y., Gottlieb, M., 2023. Zeolite performance in removal of multicomponent heavy metal contamination from wastewater. J. Hazard. Mater. 457, 131784 https://doi.org/10.1016/j.jhazmat.2023.131784.

Geng, J., Liang, Q., Yu, W., Chen, W., Lu, G., Luo, H., 2022. Enhanced removal of Cr(VI) from aqueous solutions by polymer-mediated nitrogen-rich reduced graphene oxide. J. Hazard. Mater. 436, 129184 https://doi.org/10.1016/j.jhazmat.2022.129184.

Han, G., Oh, S., Yeo, S.J., Lee, J., Lim, H., 2023. Eco-friendly polycaprolactone-bound diatomite filter for the removal of metal ions and micro/nanoplastics from water. Sci. Total Environ. 905, 166956 https://doi.org/10.1016/j.scitotenv.2023.166956.

Hethnawi, A., Manasrah, A.D., Vitale, G., Nassar, N.N., 2018. Fixed-bed column studies of total organic carbon removal from industrial wastewater by use of diatomite decorated with polyethylenimine-functionalized pyroxene nanoparticles. J. Colloid Interface Sci. 513, 28–42. https://doi.org/10.1016/j.jcis.2017.10.078.

Islam, Md.S., Rahaman, Md.S., Barbeau, B., 2023. Removal of Pb (II), Zn (II), Cu (II), and As (III) ions from water using kraft pulp-based carboxymethylated cellulose in a fixed-bed column adsorption process. J. Environ. Chem. Eng. 11, 111181 https://doi.org/10.1016/j.jece.2023.111181.

Kaur, R., Singh, J., Khare, R., Cameotra, S.S., Ali, A., 2013. Batch sorption dynamics, kinetics and equilibrium studies of Cr(VI), Ni(II) and Cu(II) from aqueous phase using agricultural residues. Appl Water Sci 3, 207–218. https://doi.org/10.1007/s13201-012-0073-y.

Kumar, A., Gupta, V., Gaikwad, K.K., 2021. Microfibrillated cellulose from pine cone: extraction, properties, and characterization. Biomass Convers. Biorefin. https://doi.org/10.1007/s13399-021-01794-2.

Kumar, M., Ambika, S., Hassani, A., Nidheesh, P.V., 2023. Waste to catalyst: role of agricultural waste in water and wastewater treatment. Sci. Total Environ. 858, 159762 https://doi.org/10.1016/j.scitotenv.2022.159762.

Lakshmipathy, R., Sarada, N.C., 2016. Methylene blue adsorption onto native watermelon rind: batch and fixed bed column studies. Desalin. Water Treat. 57, 10632–10645. https://doi.org/10.1080/19443994.2015.1040462.

Li, Y., Feng, Y., Li, H., Yao, Y., Xu, C., Ju, J., Ma, R., Wang, H., Jiang, S., 2024. Adsorption of metal ions by oceanic manganese nodule and deep-sea sediment:

behaviour, mechanism and evaluation. Sci. Total Environ. 908, 168163 https://doi.org/10.1016/j.scitotenv.2023.168163.
Liang, H., Li, Y., Zhao, X., Gao, C., Zhang, H., Geng, Z., She, D., 2022. Efficient Cr(VI) removal from wastewater by D-(+)-xylose based adsorbent: key roles of three-dimensional porous structures and oxygen groups. J. Hazard. Mater. 437, 129345 https://doi.org/10.1016/J.JHAZMAT.2022.129345.
Malik, D.S., Jain, C.K., Yadav, A.K., 2018. Heavy metal removal by fixed-bed column – a review. ChemBioEng Rev. 5, 173–179. https://doi.org/10.1002/CBEN.201700018.
Martín-Lara, M.A., Blázquez, G., Calero, M., Almendros, A.I., Ronda, A., 2016a. Binary biosorption of copper and lead onto pine cone shell in batch reactors and in fixed bed columns. Int. J. Miner. Process. 148, 72–82. https://doi.org/10.1016/j.minpro.2016.01.017.
Martín-Lara, M.A., Blázquez, G., Ronda, A., Calero, M., 2016b. Kinetic study of the pyrolysis of pine cone shell through non-isothermal thermogravimetry: effect of heavy metals incorporated by biosorption. Renew. Energy 96, 613–624. https://doi.org/10.1016/j.renene.2016.05.026.
Martín-Lara, M.A., Calero de Hoces, M., Ronda Gálvez, A., Pérez Muñoz, A., Trujillo Miranda, M.C., 2016c. Assessment of the removal mechanism of hexavalent chromium from aqueous solutions by olive stone. Water Sci. Technol. 73, 2680–2688. https://doi.org/10.2166/wst.2016.081.
Miralles, N., Valderrama, C., Casas, I., Martínez, M., Florido, A., 2010. Cadmium and lead removal from aqueous solution by grape stalk wastes: modeling of a fixed-bed column. J. Chem. Eng. Data 55, 3548–3554. https://doi.org/10.1021/je100200w.
Myers, T.G., Cabrera-Codony, A., Valverde, A., 2023. On the development of a consistent mathematical model for adsorption in a packed column (and why standard models fail). Int. J. Heat Mass Transf. 202 https://doi.org/10.1016/j.ijheatmasstransfer.2022.123660.
Radhakrishnan, K., Sethuraman, L., Panjanathan, R., Natarajan, A., Solaiappan, V., Thilagaraj, W.R., 2016. Biosorption of heavy metals from actual electroplating wastewater using encapsulated *Moringa oleifera* beads in fixed bed column. Desalin. Water Treat. 57, 3572–3587. https://doi.org/10.1080/19443994.2014.985725.
Rajoria, S., Vashishtha, M., Sangal, V.K., 2022. Treatment of electroplating industry wastewater: a review on the various techniques. Environ. Sci. Pollut. Res. https://doi.org/10.1007/s11356-022-18643-y.
Ravat, C., Monteil-Rivera, F., Dumonceau, J., 2000. Metal ions binding to natural organic matter extracted from wheat bran: application of the surface complexation model. J. Colloid Interface Sci. 225, 329–339. https://doi.org/10.1006/jcis.2000.6782.
Reshmy, R., Philip, E., Madhavan, A., Pugazhendhi, A., Sindhu, R., Sirohi, R., Awasthi, M.K., Pandey, A., Binod, P., 2022. Nanocellulose as green material for remediation of hazardous heavy metal contaminants. J. Hazard. Mater. 424, 127516 https://doi.org/10.1016/j.jhazmat.2021.127516.
Singh, V., Ram, C., 2016. Physico-chemical characterization of electroplating industrial effluents of Chandigarh and Haryana Region. J. Civ. Environ. Eng. 6 https://doi.org/10.4172/2165-784X.1000237.
Sips, R., 1948. On the structure of a catalyst surface. J. Chem. Phys. 16, 490–495. https://doi.org/10.1063/1.1746922.
Stala, Ł., Ulatowska, J., Polowczyk, I., 2021. A review of polyampholytic ion scavengers for toxic metal ion removal from aqueous systems. Water Res. 203, 117523 https://doi.org/10.1016/j.watres.2021.117523.
Stala, Ł., Ulatowska, J., Polowczyk, I., 2022. Copper(II) ions removal from model galvanic wastewater by green one-pot synthesised amino-hypophosphite polyampholyte. J. Hazard. Mater. 436, 129047 https://doi.org/10.1016/j.jhazmat.2022.129047.
Ucun, H., Bayhana, Y.K., Kaya, Y., Cakici, A., Algur, O.F., 2003. Biosorption of lead (II) from aqueous solution by cone biomass of Pinus sylvestris. Desalination 154, 233–238. https://doi.org/10.1016/S0011-9164(03)80038-3.
Valverde, A., Cabrera-Codony, A., Calvo-Schwarzwalder, M., Myers, T.G., 2024. Investigating the impact of adsorbent particle size on column adsorption kinetics through a mathematical model. Int. J. Heat Mass Transf. 218, 124724 https://doi.org/10.1016/j.ijheatmasstransfer.2023.124724.
Vera, L.M., Bermejo, D., Uguña, M.F., Garcia, N., Flores, M., González, E., 2018. Fixed bed column modeling of lead(II) and cadmium(II) ions biosorption on sugarcane bagasse. Environ. Eng. Res. 24, 31–37. https://doi.org/10.4491/eer.2018.042.
Wang, Q., Wang, Y., Yang, Z., Han, W., Yuan, L., Zhang, L., Huang, X., 2022. Efficient removal of Pb(II) and Cd(II) from aqueous solutions by mango seed biosorbent. Chem. Eng. J. Adv. 11, 100295 https://doi.org/10.1016/j.ceja.2022.100295.
Yahya, M.D., Abubakar, H., Obayomi, K.S., Iyaka, Y.A., Suleiman, B., 2020. Simultaneous and continuous biosorption of Cr and Cu (II) ions from industrial tannery effluent using almond shell in a fixed bed column. Results Eng. 6, 100113 https://doi.org/10.1016/j.rineng.2020.100113.
Zahara, I., Irfan, M.F., Zubair, M., Siddique, T., Ullah, A., 2023. Removal of divalent cations and oxyanions by keratin-derived sorbents: influence of process parameters and mechanistic studies. Sci. Total Environ. 891, 164288 https://doi.org/10.1016/j.scitotenv.2023.164288.